

Determination of Zinc Impurity Composition by Microwave Plasma Atomic Emission Spectrometry

E. V. Polyakova^{a, b, *}, Yu. N. Nomerotskaya^{a, b}, and A. I. Saprykin^{a, b}

^aNikolaev Institute of Inorganic Chemistry, Siberian Branch, Russian Academy of Sciences, Novosibirsk, 630090 Russia

^bNovosibirsk State University, Novosibirsk, 630090 Russia

*e-mail: e_polyak@niic.nsc.ru

Received February 2, 2018; revised June 13, 2018; accepted December 19, 2018

Abstract—Microwave plasma atomic emission spectrometry was used to determine 36 impurity elements in the zinc metal by a calibration method without adding the matrix element. The values of the nebulizer gas flow pressure are selected that ensure the maximum analytical signals of impurity elements. The limits of detection for most elements are 10^{-5} – 10^{-4} wt %; the error of the results of analysis is 10%. The accuracy is confirmed by the standard addition method and the analysis of standard reference samples.

Keywords: microwave plasma atomic emission spectrometry (MP AES), impurities, zinc, alloys, nebulizer flow

DOI: 10.1134/S1061934819070074

Conventional methods for determining the impurity composition are inductively coupled plasma atomic emission spectrometry (ICP AES), inductively coupled plasma mass spectrometry, and electrothermal atomization atomic absorption spectrometry [1–3]. In 2011, Agilent Technologies launched the Agilent 4100 atomic emission spectrometer with excitation of spectra in a microwave plasma, in which nitrogen is used as the plasma-forming gas. The design of the device is similar to that of ICP spectrometers, and the cost of its operation is much lower, as the necessary nitrogen enters the generator from the air. The temperature of microwave nitrogen plasma is 4500–5500 K, which is lower than the temperature of argon inductively coupled plasma. Therefore, many elements show only atomic lines as the most intense, except for alkali and alkaline-earth elements and those elements, the intense atomic lines of which overlap with the spectrum of the nitrogen plasma, while the emission spectra of the elements are simpler than those obtained in the ICP [4]. It was demonstrated that atomic emission spectrometry with spectrum excitation in microwave plasma (microwave plasma atomic emission spectrometry, MP AES) is suitable for the analysis of geological and technogenic samples after acid decomposition [5–7], biological samples [8–11], food [12–14], drinks [15, 16], natural waters [17], and leather and textile materials [10, 18]. However, there is practically no information on the MP AES analysis of objects with an inorganic matrix, for example, alloys or functional materials [19–21]. It is known that the matrix effects on the AES results can

be significant [4, 22]. Although, in general, the limits of detection in MP AES are somewhat higher than those in ICP AES [4, 23], it is interesting to evaluate the possibilities of the method for determining the impurity composition in the presence of a matrix element.

The matrix element, being present in a significant amount as compared with the impurity elements, can change the parameters of the plasma, which affects the intensity of the analytical signals. For correcting the matrix effect on the results in AES analysis, various methods are used: dilution (selection of the concentration of the matrix element in the sample), use of calibration curves with the addition of the main element, or use of the internal standard [24–26].

The purpose of this work is to study the possibility of obtaining the correct analysis results and estimate the limits of detection for impurity elements by MP AES in the presence of a matrix element with a high ionization potential, which does not form additional compounds in the plasma. Zinc having $E_{\text{ioniz}} = 9.39$ eV satisfies these requirements. As an object of analysis, we select a zinc alloy used for hot galvanizing of metals and metal products in order to prevent corrosion; the zinc concentration in the alloy is 92–99%. Technologically important impurities in the alloy are Pb, Bi, Fe, Cu, Mn, Ni, Sn, Al, Si, etc.

EXPERIMENTAL

Reagents and equipment. We used nitric acid and deionized water with a specific resistance of

≥ 18 M Ω /cm purified in an Ultrapure Water System Direct Q-3 (Millipore) to transfer zinc samples into a solution. Calibration curves were plotted using solutions of multielement reference samples (multielement standards, MESs): MES 1 (50 mg/L of Al, Ca, Cd, Fe, Mg, Mn, Na, Cr, Zn, K, and P and 10 mg/L of Li), MES 2 (50 mg/L of B, V, Bi, Ga, In, Co, Cu, Ni, Si, and Ti), MES 3 (50 mg/L of As, Sn, Rb, Pb, Se, Sb, and Te; 20 mg/L of Ba and Sr; 10 mg/L of Be, Ag, and Au; and 5 mg/L of Hg), and MES 4 (50 mg/L of W, Hf, Mo, Nb, Re, Ta, and Zr) (Skat, Russia). The reference samples were diluted with 1% (vol) nitric acid.

The measurements were performed using a 4100 MPAES spectrometer (Agilent Technologies) equipped with a conventional magnetron with a frequency of 2450 MHz, a Czerny–Turner monochromator, and a CCD detector thermostated at 0°C using a Peltier device. To obtain nitrogen, a 4107 Nitrogen Generator (Agilent Technologies) generator was used. The plasma power was 1 kW; the plasma was observed in an axial direction in the “zero” position. An inert OneNeb nebulizer (Agilent) and a Cyclonic Spray Chamber, Double Pass chamber (Agilent) were used to inject the samples. The plasma stabilization time was 15 s; the number of sample injections was 3; the number of pixels for processing analytical signals was 1.

Spectra were processed using the Agilent MP Expert software (ver. 1.5.2.7948). In the “auto” spectral peak processing mode, the software simulates the peak shape based on the spectra of a “blank” sample and calibration solutions; in “off-peak” modes, background signal metering points are manually selected by the user.

Dissolution of samples. A portion of zinc weighing 250 mg was placed in a polypropylene test tube; 1.5 mL of nitric acid (1 : 1) was added dropwise. After cooling to room temperature, the resulting solution was diluted and analyzed. A blank solution was prepared similarly.

It is known that microwave plasma is very sensitive to the salt composition of the injected solution. The manufacturer does not recommend spraying solutions with a total salt concentration above 2%. In this regard, we additionally diluted the sample 20-fold; that is, the concentration of the matrix did not exceed 1%. To determine the elements with the levels of 0.01–0.1 wt % in the sample, we used dilution by 50 and 200 times. The concentration of components in the solution was determined from calibration curves plotted using multielement reference samples without adding the matrix element.

One of the parameters affecting the magnitude of the analytical signal is the nebulizer gas flow pressure, which mainly determines the residence time of the sample solution aerosol in the plasma. The nebulizer pressure was varied in the working range from 80 to

240 kPa with an interval of 40 kPa to obtain the maximum analytical signal. For this purpose, solutions of multielement reference samples with a concentration of 10 mg/L were sprayed into the plasma. The intensity of the analytical signals obtained at various pressures was normalized to the intensity at a minimum gas pressure of 80 kPa.

RESULTS AND DISCUSSION

Optimization of nebulizer gas flow pressure. The analytes can be divided into two groups by the nature of the change in the analytical signal with increasing pressure of the nebulizer flow: (1) the relative intensity increases with increasing gas flow pressure (Al, Ba, Ca, Cr, Fe, Li, Mg, Mn, Na, K, Ga, Rb, Mo, Sn, Re, Pb, and Sr; Figs. 1a–1d) and (2) the dependence reaches a plateau or has a maximum at a medium pressure (As, B, Bi, Cd, Cu, Co, Ni, Sb, Si, Ta, Te, Ti, Hf, Nb, and Zn; Figs. 1d–1h). The selected values of pressure and the energy characteristics of the lines are given in Table 1. The nebulizer flow pressure affects the intensity ratio of most elements significantly; the change can amount several times. The first group includes elements with atomic lines with low excitation energy, as well as ionic lines with a sum of ionization and excitation energies from 5.96 to 7.93 eV (except for Mg II 279.553 with E_{ex} 12.07 eV). It is known [27] that an increase in the flow rate leads to a change in the plasma temperature by several hundred degrees in the “zero” observation position; in addition, the electron density increases by two or three times. The presence of ionic lines, the intensity of which does not decrease at the maximum pressure of the nitrogen flow, indicates the effective evaporation of the increased number of aerosol droplets. The excitation energies of the atomic lines of the second group of elements intersect with those of the first group. Apparently, the nature of the element plays a role. The atomic lines of nonmetals, as well as metals forming refractory compounds, are in the range of 4.5–6.6 eV. Ionic lines with a sum of energies greater than 9 eV belong to elements forming refractory compounds, such as Zr, Hf, Ti, Nb, and Be. Taking into account the plasma temperature (approximately 4500 K [27]), it can be assumed that for the elements of the second group, the decisive factors are the lack of plasma energy for the conversion of elements into atomic form; the increased electron density, which decreases the intensity of ionic lines; and the local decrease in temperature with an increasing amount of solvent, accompanying the increase in the nebulizer flow pressure. We note for comparison that in the ICP, the medium value of the nebulizer flow rate is optimal for all elements, while the plasma power has a crucial role [28], especially for atomic lines with $E_{\text{ex}} > 5$ eV and $E_{\text{ioniz}} > 10$ eV.

Calibration dependences, signal processing, account of background signal. In contrast to ICP, the calibra-

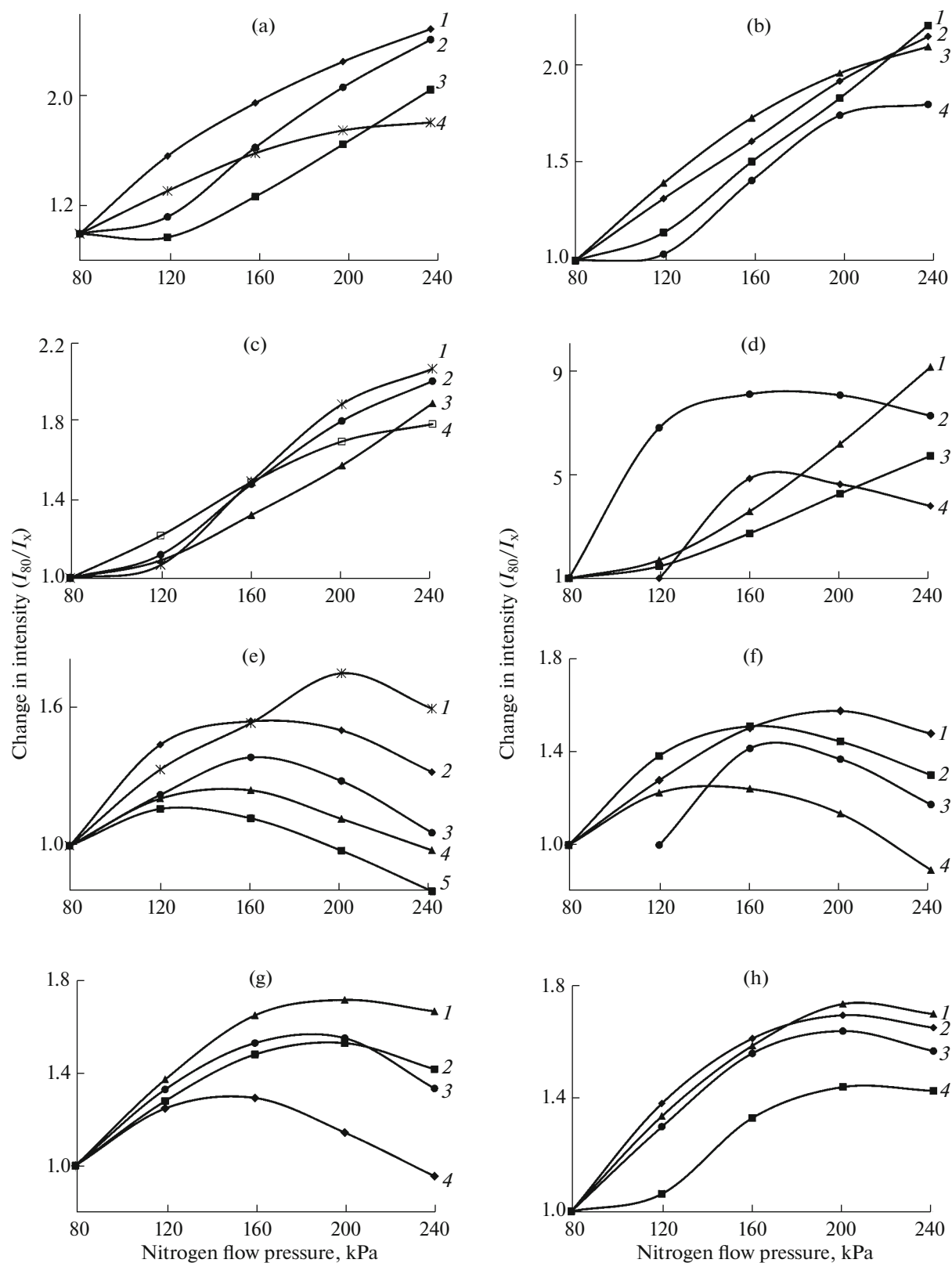


Fig. 1. Change in the magnitude of the analytical signal with increasing nitrogen flow pressure: (a) (1) Sn 317.505, (2) Na 588.995, (3) Al 393.152, and (4) Re 346.046; (b) (1) Ga 417.204, (2) Mo 379.825, (3) Fe 371.993, and (4) Sr 407.771; (c) (1) Ba 455.403, (2) Li 670.784, (3) Cr 425.433, and (4) Mg 285.213; (d) (1) Rb 780.027, (2) Sb 231.147, (3) K 766.491, and (4) As 193.695; (e) (1) Bi 306.772, (2) Cd 228.802, (3) Hf 339.980, (4) Be 234.861, and (5) B 249.772; (f), (1) Ti 334.941, (2) Nb 309.418, (3) Te 214.281, and (4) Si 251.611; (g) (1) W 400.875, (2) V 309.311, (3) Zr 343.823, and (4) Ta 268.473; and (h) (1) Co 345.351, (2) Ni 352.454, (3) Cu 324.754, and (4) Ca 393.366.

Table 1. Group assignment of the lines of analytes depending on the reaction of the normalized intensity to the increase in the nitrogen flow pressure

Relative intensity increases			Relative intensity reaches a plateau or has a pronounced maximum		
element, analytical line, nm	optimal gas flow pressure, kPa	$E_{\text{ex}} + E_{\text{ioniz}}, \text{ eV}$	element, analytical line, nm	optimal gas flow pressure, kPa	$E_{\text{ex}} + E_{\text{ioniz}}, \text{ eV}$
Rb I 780.027	240*	1.59	V I 437.923	200*	3.13
Cr I 425.43	240	2.91	W I 400.875	200*	3.45
Ga I 417.204	240*	3.07	Ni I 341.476	200*	3.65
Mn I 403.076	240	3.08	Cu I 324.754	200*	3.82
Al I 396.152	240	3.14	Co I 340.512	200*	4.07
Mo I 386.410	240	3.20	Bi I 223.061	180	5.55
Fe I 371.993	240*	3.33	Te I 238.578	160*	—
Re I 346.046	240	3.58	Cd I 228.802	160*	5.41
Sn I 303.412	240	4.30	Sb I 217.581	160*	5.69
Pb I 405.781	240	4.38	As I 228.812	160*	6.77
K I 766.491	240	5.96	Ta I 271.467	140	4.56
Na I 588.995	240	7.25	B I 249.772	140*	4.96
Li I 670.784	240	7.27	Si I 288.158	140	5.08
Ba II 455.403	240	7.93	Ca II 393.366	200*	9.26
Sr II 407.771	240*	8.73	Zr II 343.823	200*	10.53
Mg II 279.553	240	12.07	Ti II 334.941	200*	10.56
			Hf II 356.166	160*	10.08
			Nb II 316.340	160*	11.18
			Be II 313.042	140*	13.28

* Pressure values different from those recommended by Agilent.

tion dependences for most elements (the dependence of intensity on concentration) are nonlinear and are approximated by second-order curves, covering ranges of two orders of magnitude. Therefore, to plot the calibration dependence, it is necessary to obtain 4–6 points (Table 2).

We aimed at accounting for the modified background signal in the presence of the matrix element properly and considered various options provided by the software: “auto,” “left–right,” “left of the peak,” and “right of the peak.” The results of the standard addition experiment served as the selection criterion, in which a solution of a multielement reference sample was added to a solution of a zinc sample diluted 20–50 times. Several lines were considered for each element; the most intense of those and free from overlays of the matrix element and the main impurities—Pb, Fe, Cu, Bi, Ni, and Sn—was selected (Table 2). For half of the selected lines, the background signal is almost unchanged and is satisfactorily taken into account in the “auto” mode. More significant changes in the background signal are well handled by selecting accounting limits on both sides of the peak (“left–right” mode). Only the lines of Be at 313.042 nm, Re

at 346.046 nm, Sb at 217.581 nm, and Sn at 303.412 nm require one-way accounting of the background signal. The results of the spiking experiment for the selected lines and options for accounting for the background signal are listed in Table 3. The recovery (the found-to-added ratio, taking into account the concentration in the sample solution) is 0.90–1.08 for most elements, and 0.79–1.26 for As, B, Ga, Si, and Ti.

Verification of accuracy. To verify the accuracy of measurements, a standard sample of zinc composition with impurity concentrations of $n \times 10^{-3}\%$ was additionally analyzed (Table 4). The results agree well with the certified values, which indicates the absence of a significant systematic error. The analysis error does not exceed 10% for two parallel determinations. The limits of detection for impurities in zinc, calculated by the $3s$ criterion, were $n \times 10^{-6}$ – 10^{-3} wt %.

CONCLUSIONS

It is shown that nebulizer flow pressure significantly affects the magnitudes of the analytical signals of the elements in MP AES. The maximum intensities

Table 2. Conditions for the MPAES determination of impurities and their limits of detection in zinc

Element, analytical line, nm	Calibration function	Calibration range, mg/L	Accounting for background signal	Detection limit, wt %	Lower limit of the regulated range, wt % [29]
Al 396.152	Rational	0.31–10	Auto	2×10^{-5}	1×10^{-3}
As 228.812	Rational	0.16–5.0	Left–right	4×10^{-3}	
B 249.772	Rational	0.16–5.0	Auto	2×10^{-5}	
Ba 455.403	Rational	0.06–2.0	Left–right	1×10^{-5}	
Be 313.042	Linear	0.031–1.00	Right of the peak	1×10^{-5}	
Bi 223.061	Rational	0.16–5.0	Auto	2×10^{-5}	
Ca 393.366	Rational	0.31–10	Left–right	1×10^{-3} (CE)	
Cd 228.802	Rational	0.31–10	Auto	7×10^{-4}	1×10^{-3}
Co 340.512	Rational	0.16–5.0	Left–right	2×10^{-4}	
Cr 425.433	Rational	0.31–10	Auto	2×10^{-5}	
Cu 324.754	Linear	0.31–10	Auto	1×10^{-5}	5×10^{-4}
Fe 371.993	Rational	0.31–10	Auto	7×10^{-5}	1×10^{-3}
Ga 417.204	Rational	0.16–5.0	Left–right	7×10^{-4}	
Hf 356.166	Rational	0.31–5.0	Left–right	1×10^{-3}	
In 410.176	Rational	0.16–5.0	Left–right	2×10^{-4}	
K 766.491	Linear	0.31–5.0	Left–right	4×10^{-5}	
Li 670.784	Linear	0.062–5.0	Auto	4×10^{-6}	
Mg 279.553	Linear	0.31–10	Auto	2×10^{-4}	
Mn 403.076	Rational	0.31–10	Auto	4×10^{-5}	
Mo 386.410	Rational	0.16–5.0	Auto	7×10^{-4}	
Na 588.995	Linear	0.31–10	Auto	6×10^{-4}	
Nb 316.340	Rational	0.31–5.0	Auto	1×10^{-3}	
Ni 341.476	Linear	0.15–5.0	Left–right	1×10^{-5}	
Pb 405.781	Rational	0.15–5.0	Left–right	3×10^{-4}	1×10^{-3}
Rb 780.02	Linear	0.15–5.0	Left–right	1×10^{-4}	
Re 346.046	Rational	0.15–5.0	Left of the peak	1×10^{-4}	
Sb 217.581	Rational	0.15–5.0	Left of the peak	1×10^{-3}	1×10^{-3}
Si 288.158	Rational	0.15–5.0	Left–right	1×10^{-3}	
Sn 303.412	Rational	0.15–5.0	Left of the peak	1×10^{-3}	7×10^{-4}
Sr 407.771	Linear	0.063–2.0	Auto	1×10^{-6}	
Ta 271.467	Rational	0.31–5.0	Auto	1×10^{-3}	
Te 238.578	Rational	0.15–5.0	Auto	6×10^{-3}	
Ti 334.941	Rational	0.15–5.0	Auto	2×10^{-5}	
V 437.923	Rational	0.15–5.0	Auto	2×10^{-5}	
W 400.875	Rational	0.15–5.0	Left–right	2×10^{-4}	
Zr 343.823	Linear	0.15–5.0	Left–right	1×10^{-5}	

Abbreviations: CE, control experiment.

Table 3. Results (mg/L) of determination of elements in zinc solution by the standard addition method for selected analytical lines

Element, analytical line, nm	Added	Found	Recovery	Element, analytical line, nm	Added	Found	Recovery
Al 396.152	0.417	0.401	0.96	Mo 386.410	0.625	0.57	0.91
	2.75	2.62	0.95		1.25	1.22	0.98
As 228.812	1.64	1.82	1.1	Na 588.995	0.315	0.311	0.99
	1.06	1.31	1.2		2.50	2.49	0.99
B 249.772	0.0782	0.0684	0.88	Nb 316.340	1.00	0.884	0.88
	1.25	1.06	0.85		2.50	2.44	0.98
Ba 455.403	0.25	0.23	0.92	Ni 341.476	2.06	1.99	0.97
	0.50	0.48	0.96		2.86	2.87	1.00
Be 313.042	0.136	0.103	0.76	Pb 405.781	6.51	6.72	0.93
	0.25	0.24	0.96		5.94	6.13	1.03
Bi 223.061	0.495	0.530	1.07	Rb 780.027	1.00	0.960	0.96
	2.08	2.08	1.00		2.50	2.45	0.98
Ca 393.366	0.183	0.175	0.96	Re 346.046	0.87	0.74	0.85
	2.52	2.30	0.92		1.44	1.31	0.91
Cd 228.802	0.173	0.165	0.95	Sb 217.581	0.70	0.80	1.14
	2.50	2.35	0.94		1.32	1.27	0.96
Co 340.512	0.156	0.144	0.92	Si 288.158	0.166	0.195	1.18
	1.25	1.20	0.96		1.29	1.23	0.95
Cr 425.433	0.173	0.174	1.01	Sn 303.412	1.92	1.91	1.00
	2.52	2.64	1.05		3.08	3.16	1.03
Cu 324.754	0.234	0.229	0.98	Sr 407.771	0.25	0.23	0.92
	1.45	1.39	0.96		0.50	0.47	0.94
Fe 371.993	0.784	0.843	1.08	Ta 271.467	1.00	0.979	0.98
	0.940	0.980	1.04		2.50	2.64	1.06
Ga 417.204	0.172	0.158	0.92	Te 238.578	1.00	1.35	1.4
	1.27	1.14	0.90		2.5	2.71	1.08
Hf 356.166	1.00	1.12	1.12	Ti 334.941	0.156	0.197	1.3
	2.50	2.41	0.96		1.25	1.23	0.99
K 766.491	0.168	0.178	1.06	V 437.923	0.0839	0.0814	0.97
	0.324	0.328	1.01		1.26	1.21	0.96
Li 670.784	0.064	0.05688	0.88	W 400.875	0.625	0.60	0.96
	0.502	0.457	0.91		1.25	1.21	0.97
Mg 279.553	0.313	0.282	0.91	Zr 343.823	1.00	0.956	0.96
	2.50	2.22	0.89		2.50	2.36	0.94
Mn 403.076	0.387	0.409	1.06				
	2.69	2.67	0.99				

Table 4. Results (wt %) of the analysis of VSZ1-4 and VSZ1-2 standard samples of zinc composition ($n = 3$, $P = 0.95$)

Element	VSZ1-4		VSZ1-2	
	certified	found	certified	found
As	$(2.8 \pm 0.3) \times 10^{-3}$	$<4 \times 10^{-3}$	$(4.9 \pm 0.6) \times 10^{-4}$	$<4 \times 10^{-3}$
Cd	$(2.42 \pm 0.25) \times 10^{-3}$	$(2.6 \pm 0.4) \times 10^{-3}$	$(2.9 \pm 0.3) \times 10^{-4}$	$(2.4 \pm 0.3) \times 10^{-4}$
Cu	$(2.38 \pm 0.25) \times 10^{-3}$	$(2.3 \pm 0.3) \times 10^{-3}$	$(5.4 \pm 0.6) \times 10^{-4}$	$(5.7 \pm 0.6) \times 10^{-4}$
Fe	$(7.4 \pm 0.8) \times 10^{-3}$	$(7 \pm 1) \times 10^{-3}$	$(5.3 \pm 0.5) \times 10^{-4}$	$(5.6 \pm 0.6) \times 10^{-4}$
Mg	$(2.7 \pm 0.3) \times 10^{-3}$	$(2.4 \pm 0.4) \times 10^{-3}$	$(1.1 \pm 0.2) \times 10^{-4}$	$<2 \times 10^{-4}$
Pb	$(4.9 \pm 0.4) \times 10^{-3}$	$(4.3 \pm 0.6) \times 10^{-3}$	$(1.12 \pm 0.10) \times 10^{-3}$	$(1.1 \pm 0.3) \times 10^{-3}$
Sb	$(1.1 \pm 0.7) \times 10^{-2}$	$(1.3 \pm 0.2) \times 10^{-3}$	$(1.18 \pm 0.15) \times 10^{-3}$	$(1.5 \pm 0.2) \times 10^{-3}$
Sn	$(2.06 \pm 0.18) \times 10^{-3}$	$(2.2 \pm 0.3) \times 10^{-3}$	$(5.9 \pm 0.2) \times 10^{-4}$	$<1 \times 10^{-3}$

of the analytical signals are obtained at the maximum pressure or in the middle of the working pressure range, depending on the sum of excitation and ionization energies and the nature of the element. A possibility of determining 36 elements, being impurities in the zinc metal, at a level of 10^{-6} – 10^{-3} wt % is demonstrated. A wide range of determined impurities makes it possible to calculate the concentration of the main element from the difference between 100% and the total concentration of impurities in one analysis. The method can be recommended for determining the composition of zinc-based alloys and technical zinc as an alternative to ICP AES or direct current arc atomic emission spectrometry [29].

FUNDING

This work was supported by the Federal Agency for Scientific Organizations of the Russian Federation.

REFERENCES

1. *Inorganic Chemical Biology: Principles, Techniques and Applications*, Gasser, G., Ed., Chichester: Wiley, 2014.
2. *Handbook of Mineral Elements in Food*, de la Guardia, M. and Garrigues, S., Eds., Chichester: Wiley, 2015.
3. *Handbook of Trace Analysis. Fundamentals and Applications*, Baranowska, I., Ed., Springer, 2016.
4. Jankowski, K.J. and Reszke, E., Microwave induced plasma analytical spectrometry, *RSC Analytical Spectroscopy Monographs*, Cambridge: The Royal Soc. Chem., 2011, no. 12.
5. Helmecci, E., Wang, Y., and Brindle, I.D., *Talanta*, 2016, vol. 160, p. 521.
6. Zhdanov, P.A., Seregin, I.F., Bol'shov, M.A., Volkov, A.I., and Seregin, A.N., *Inorg. Mater.*, 2016, vol. 52, p. 1431.
7. Balogh, Z., Harangi, S., Gyulai, I., Braun, M., Hubay, K., Tóthmérész, B., and Simon, E., *Environ. Sci. Pollut. Res.*, 2017, vol. 24, p. 4851.
8. Karlsson, S., Sjöberg, V., and Ogar, A., *Talanta*, 2015, vol. 135, p. 124.
9. Simon, E., Kis, O., Jakab, T., Kolozsvári, I., Málnás, K., Harangi, S., Baranyai, E., Miskolczi, M., Tóthmérész, B., and Dévai, G., *Ecotoxicol. Environ. Saf.*, 2017, vol. 136, p. 55.
10. Zhao, Y., Li, Z., Ross, A., Huang, Z., Chang, W., Ouyang, K., Chen, Y., and Wu, C., *Spectrochim. Acta, Part B*, 2015, vol. 112, p. 6.
11. Harangi, S., Baranyai, E., Fehér, M., Tóth, C.N., Herman, P., Stündl, L., Fábrián, I., Tóthmérész, B., and Simon, E., *Biol. Trace Elem. Res.*, 2017, vol. 177, p. 187.
12. Ozbek, N. and Akman, S., *Food Chem.*, 2016, vol. 192, p. 295.
13. Ozbek, N. and Akman, S., *Food Chem.*, 2016, vol. 200, p. 245.
14. Gallego Ríos, S.E., Peñuela, G.A., and Ramírez Botero, C.M., *Food Anal. Methods*, 2017, vol. 10, p. 3407.
15. Ozbek, N. and Akman, S., *LWT—Food Sci. Technol.*, 2015, vol. 61, p. 532.
16. Ozbek, N., Koca, M., and Akman, S., *Food Anal. Methods*, 2016, vol. 9, p. 2246.
17. Eken, M.D. and Akman, B., *Fresenius Environ. Bull*, 2017, vol. 26, p. 4845.
18. Sungur, Ş. and Gülmez, F., *J. Spectrosc.*, 2015, vol. 2015, 640271. www.hindawi.com/journals/jspec/2015/640271/. Accessed September 7, 2017.
19. Hettipathirana, T.D., *J. Anal. At. Spectrom.*, 2013, vol. 28, p. 1242.
20. Feng, X.-J., *Metall. Anal.*, 2014, vol. 34, p. 58.
21. Amorin, A., Direct determination of Al, B, Co, Cr, Mo, Ti, V and Zr in HF acid-digested nickel alloy using the Agilent 4210 Microwave Plasma-Atomic Emission Spectrometer, Agilent Technologies, 2016, publ. no. 5991-7283EN. www.agilent.com/cs/library/applications/5991-7283EN.pdf. Accessed September 7, 2017.

22. Li, W., Simmons, P., Shrader, D., Herrman, T.J., and Dai, S.Y., *Talanta*, 2013, vol. 112, p. 43.
23. Bashilov, A. and Rogova, O., *Analitika*, 2013, no. 5, p. 48. http://www.j-analytics.ru/files/article_pdf/3/article_3881_102.pdf. Accessed September 7, 2017.
24. Todolí, J.L., Gras, L., Hernandis, V., and Mora, J., *J. Anal. At. Spectrom.*, 2002, vol. 17, p. 142.
25. Donati, G.L., Amais, R.S., and Williams, C.B., *J. Anal. At. Spectrom.*, 2017, vol. 32, p. 1283.
26. Dubuisson, C., Poussel, E., and Mermet, J.M., *J. Anal. At. Spectrom.*, 1998, vol. 13, p. 1265.
27. Goncalves, D.A., McSweeney, T., and Donati, G.L., *J. Anal. At. Spectrom.*, 2016, vol. 31, p. 1097.
28. Tsygankova, A.R., Makashova, G.V., and Shelpakova, I.R., *Metody Ob'ekty Khim. Anal.*, 2012, vol. 7, no. 3, p. 138. http://www.moca.net.ua/12/3/pdf/07032012_138-142.pdf. Accessed September 7, 2017.
29. *GOST (State Standard) 17261-2008: Zinc. Methods of Atomic-Emission Spectral Analysis*, Moscow: Standartinform, 2016.

Translated by O. Zhukova